Molecular Crystals and Liquid Crystals

ISSN: 1542-1406 (Print) 1563-5287 (Online) Journal homepage: http://www.tandfonline.com/loi/gmcl20

Investigation of improved PV parameters through AMPS-1D in micromorph tandem solar cells with a microcrystalline tunnel recombination junction

Fatima Maachou, Baya Zebentout, Asmaa Bensmain, Zineb Benamara & Tayeb Mohammed Brahim

To cite this article: Fatima Maachou, Baya Zebentout, Asmaa Bensmain, Zineb Benamara & Tayeb Mohammed Brahim (2016) Investigation of improved PV parameters through AMPS-1D in micromorph tandem solar cells with a microcrystalline tunnel recombination junction, Molecular Crystals and Liquid Crystals, 627:1, 29-37, DOI: 10.1080/15421406.2015.1137117

To link to this article: http://dx.doi.org/10.1080/15421406.2015.1137117

Published online: 13 May 2016.

MOL. CRYST. LIQ. CRYST.
2016, VOL. 627, 29–37
http://dx.doi.org/10.1080/15421406.2015.1137117

Taylor & Francis
Taylor & Francis Group

Investigation of improved PV parameters through AMPS-1D in micromorph tandem solar cells with a microcrystalline tunnel recombination junction

Fatima Maachou[a], Baya Zebentout[a], Asmaa Bensmain[a], Zineb Benamara[a], and Tayeb Mohammed Brahim[b]

[a]Applied Microelectronic Laboratory, Faculty of Technology, University of Sidi Bel Abbes, Algeria; [b]IETR-Microelectronic Group, Rennes Cedex, France

ABSTRACT

The quest of higher conversion efficiencies of solar cells has led to the improvement of material properties and the design of new structures for a better use of the solar spectrum. One of the most promising thin-film silicon solar cell concepts is "Micromorph" tandem solar cells consisting of a microcrystalline silicon bottom subcell and an amorphous silicon top subcell. In this paper, a micromorph tandem solar cell (a-Si:H/μc-Si:H) with an intermediate microcrystalline tunnel recombination junction (TRJ) has been designed and analyzed by simulations using AMPS-1D (Analysis of Microelectronic and Photonic Structures) device simulator. A higher efficiency for the micromorph tandem has been achieved by optimizing each subcell and the TRJ. The open-circuit voltage V_{OC} is improved and it is nearly the sum of the V_{OC}s of the two corresponding subcells. However, the fill factor FF and short-circuit current J_{SC} are lower in comparison to the single amorphous solar cells. The spectral response behavior of the micromorph tandem has shown better utilization of solar spectrum.

KEYWORDS

Thin-film silicon; Hydrogenated amorphous silicon; Hydrogenated microcrystalline silicon; Micromorph tandem solar cells; Tunnel recombination junction

1. Introduction

Materials for thin-film silicon solar cell technology are either amorphous, microcrystalline or both. Hydrogenated amorphous silicon (a-Si:H) has always been associated with low efficiencies with further efficiency losses due to the light-induced degradation, or the so-called Staebler-Wronski effect (SWE). Therefore much effort has gone into increasing the conversion efficiency and stability in hydrogenated amorphous silicon (a-Si:H) single junction p-i-n solar cells [1,2].

The multijunction concept constitutes a practical solution for improving the efficiency and the stability of amorphous silicon based solar cells. It consists of a stack of two or more single junction solar cells with thin intrinsic layers (i-layers). Indeed, the thin i-layer is less prone to light-induced degradation, so using a stack of subcells results in a same light absorption as in case of the conventional amorphous single junction. We talk about a tandem or double junction solar cell in case of a stack of two subcells and a stack of three subcells is called triple junction [3].

CONTACT Fatima Maachou fat_maachou@yahoo.fr; Baya Zebentout b_zebentout@yahoo.fr Applied Microelectronic Laboratory, Faculty of Technology, University of Sidi Bel Abbes, 22000, Algeria.

With the development of hydrogenated microcrystalline silicon (μc-Si:H) based solar cells, a real tandem cell structure based on silicon alone was developed. μc-Si:H with low bandgap (1.14 eV) can be combined advantageously with a-Si:H which has a high bandgap (1.72 eV). These so-called micromorph tandem solar cells consist of an amorphous silicon top cell and a microcrystalline silicon bottom cell [4]. The concept was introduced by Institute for Microtechnology of Neuchâtel (IMT), based on VHF-GD (Very High Frequency-Glow Discharge) deposition method [2]. The implementation of two materials with different optical bandgaps makes better use of the solar spectrum and thus achieves higher conversion efficiencies [5]. Furthermore, as microcrystalline silicon cells do not show any light-induced degradation effect [6,7], more stabilized efficiencies could be obtained with micromorph tandem solar cells.

For proper operation, the micromorph tandem device requires a good ohmic contact between the top and bottom cells. To meet this requirement, an n-p junction or so-called a tunnel recombination junction (TRJ) is implemented between the adjacent subcells [8].

The aim of this paper is to analyze and optimize a tandem micromorph structure with a microcrystalline TRJ by using AMPS-1D software intended for non crystalline materials simulation [9]. Detailed numerical simulations will be used to gain insight on the operation of this cell and to explain the observed improvement in cell performance.

2. Device structure

The micromorph tandem solar cell with a microcrystalline TRJ illustrated in Fig. 1 has been simulated and analyzed to determine the optimum structure for a better efficiency. At first, one needs to analyze the performance of the single component cells individually (Fig. 2) in terms of the open- circuit voltage (V_{OC}), the short-circuit current (J_{SC}), the fill factor (FF) and the efficiency (η) in order to observe the improvement made by micromorph tandem cell.

Each cell is deposited on a transparent conducting oxide (front TCO) coated glass substrate in p-i-n or "superstrate" configuration. In this configuration, the light enters at the substrate side and travels through the front TCO and p- doped layer. The front TCO should have a low resistivity as well as a high transmittance in visible and near-infrared range. The metal (Ag) and back TCO form the back reflector (BR). The silver acts also as back contact for the solar cell. The back TCO acts as a diffusion barrier and protects the silicon layers from the metallic atoms [10]. The i-layer or absorber layer is sandwiched between p- and n- doped layers, so that an electric field is built over the i-layer which separates the photogenerated electron-hole pairs from each other and drifts them to the doped layers where they are collected by electrical contacts. The doped layers should be as thin as possible in order to minimize the electric and optical losses. In case of the a-Si:H p-i-n solar cell, a wide optical bandgap p-type a-SiC:H material is implemented as a window layer in order to enhance the light transmission[11], reduce the optical losses and improve the open-circuit voltage [12].

In the micromorph tandem solar cell, the electrons and holes photogenerated in the top and bottom i-layers, respectively, should recombine in order to prevent an accumulation of charge in the interface which would disturb the field distribution leading to a reduction of the built-in potential over the i-layer which results in degraded cell performances [13]. Therefore, the two subcells have to be electrically connected in series by a tunnel recombination junction which consists of heavily n and p doped layers. The junction will allow an ohmic and low resistive electrical connection between adjacent subcells, combined with low parasitic optical absorption for improving the carrier transport [14]. It should promote carrier

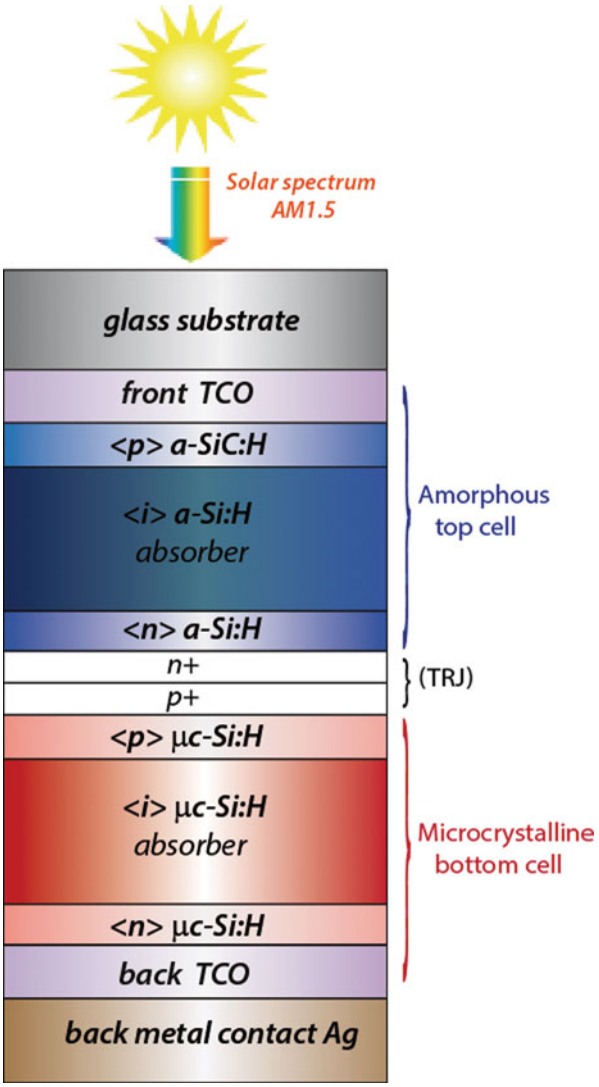

Figure 1. Schematic structure of micromorph tandem solar cell.

recombination, so a sufficiently high density of midgap defects are required in order to maintain a high recombination rate [8].

The design parameters injected into AMPS-1D are given in Tables 1 and 2. Most material parameters are provided by AMPS-1D references.

3. Results and discussion

3.1. *Amorphous and microcrystalline p-i-n cells*

Figure 3 shows the J-V characteristics under AM 1.5 illumination for an a-Si:H p-i-n solar cell with the corresponding output parameters for i-layer thickness varied in the range of 100–500 nm. V_{OC} and FF decrease with increasing the i-layer thickness. The decrease of V_{OC} is probably related to the associated increase of defect densities [12]. Higher defects affect the electric field and carrier collection yielding in poor V_{OC} [15]. From our results, the best

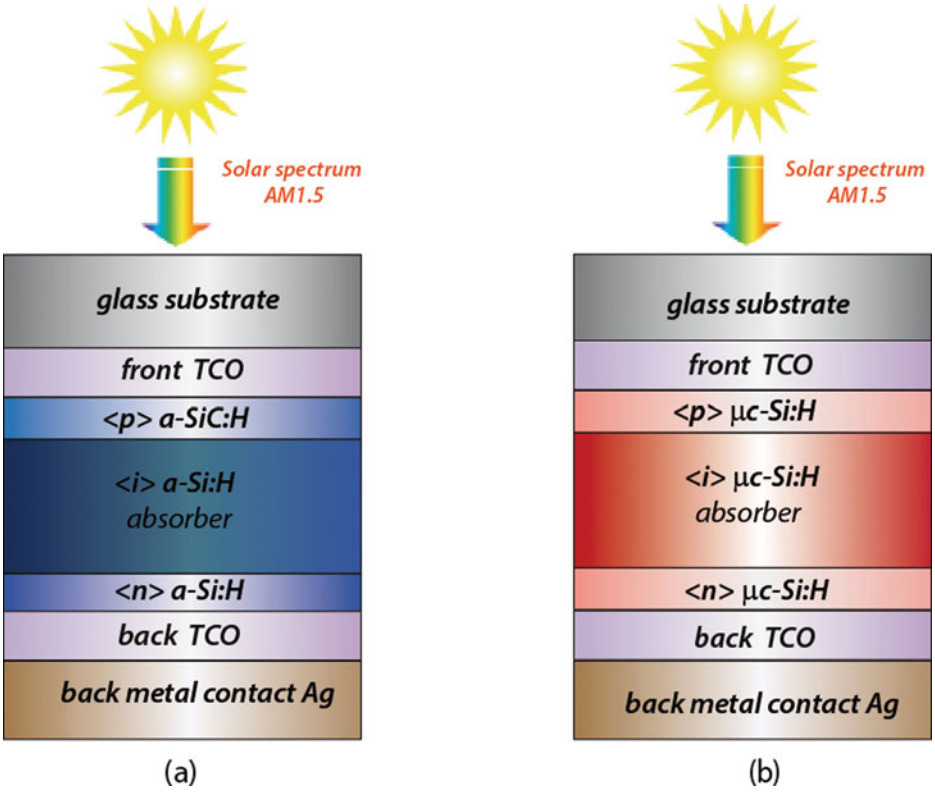

Figure 2. Schematic structure of single junctions (a) a-Si:H p-i-n solar cell (b) μc-Si:H p-i-n solar cell.

efficiency of 8.83% has been reached with $V_{OC} = 923$ mV, FF = 0.7 and $J_{SC} = 13.7$ mA/cm^2 for i-layer thickness of 200 nm. Because of the Staebler-Wronski effect in amorphous cells, the i- layer thickness has to be lower than 300 nm.

Figure 4 illustrates the quantum efficiency (QE) with various i-layer thicknesses. This shows that the hydrogenated amorphous silicon single junction absorbs short wavelengths

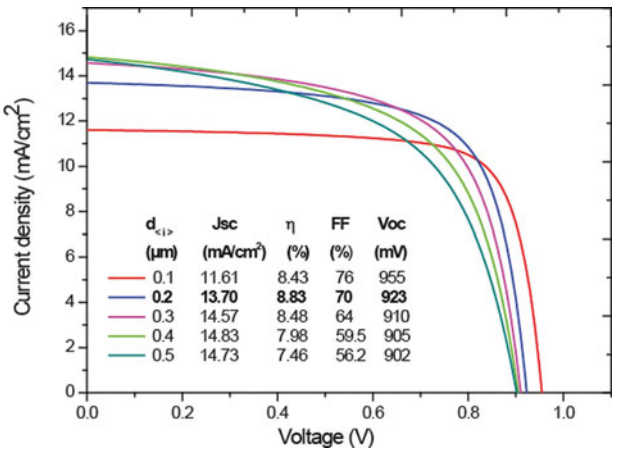

Figure 3. J-V curve under AM 1.5 illumination for a-Si:H p-i-n solar cell for different i-layer thicknesses with the output parameters.

Table 1. The set of input parameters used in the simulation.

Materials/Parameters	p-a-SiC:H	i-a-Si:H	n-a-Si:H	p-μc-Si:H	i-μc-Si:H	n-μc-Si:H	n^+ (TRJ)	p^+ (TRJ)
ε_r	11.9	11.9	11.9	11.9	11.9	11.9	11.9	11.9
χ (eV)	3.7	3.8	3.8	4	4	4	4	4
E_G (eV)	1.96	1.82	1.82	1.14	1.14	1.14	1	1
E_{opt} (eV)	1.88	1.72	1.72	1.14	1.14	1.14	1	1
d (nm)	5	—	10	20	—	20	5	5
N_D (cm^{-3})	0	1×10^{15}	1×10^{19}	0	1×10^{15}	1×10^{19}	1×10^{20}	0
N_A (cm^{-3})	1×10^{19}	0	0	1×10^{19}	0	0	0	1×10^{20}
μ_e (cm^2/Vs)	5	20	10	20	140	20	20	2
μ_h (cm^2/Vs)	0.5	2	1	2	48	2	20	2
N_C (cm^{-3})	2.5×10^{20}	2.5×10^{20}	2.5×10^{20}	3×10^{19}	3×10^{19}	3×10^{19}	3×10^{19}	3×10^{19}
N_V (cm^{-3})	2.5×10^{20}	2.5×10^{20}	2.5×10^{20}	2×10^{19}	2×10^{19}	2×10^{19}	2×10^{19}	2×10^{19}
E_D/E_A (eV)	0.12/0.07	0.05/0.03	0.05/0.03	0.03/0.01	0.03/0.01	0.03/0.01	0.03/0.01	0.03/0.01
G_{DO}/G_{AO} (cm^{-3} eV^{-1})	1×10^{21}	1×10^{21}	1×10^{21}	1×10^{20}	1×10^{19}	1×10^{20}	1×10^{20}	1×10^{20}
σ_{de} (cm^2) (tails)	1×10^{-15}	1×10^{-15}	1×10^{-15}	1×10^{-15}	1×10^{-15}	1×10^{-15}	1×10^{-15}	1×10^{-15}
σ_{dh} (cm^2) (tails)	1×10^{-17}	1×10^{-17}	1×10^{-17}	1×10^{-17}	1×10^{-17}	1×10^{-17}	1×10^{-17}	1×10^{-17}
σ_{ae} (cm^2) (tails)	1×10^{-17}	1×10^{-17}	1×10^{-17}	1×10^{-17}	1×10^{-17}	1×10^{-17}	1×10^{-17}	1×10^{-17}
σ_{ah} (cm^2) (tails)	1×10^{-15}	1×10^{-15}	1×10^{-15}	1×10^{-15}	1×10^{-15}	1×10^{-15}	1×10^{-15}	1×10^{-15}
N_{DG} (cm^{-3})	2.5×10^{18}	5×10^{16}	1×10^{18}	—	—	—	—	—
N_{AG} (cm^{-3})	2.5×10^{18}	5×10^{16}	1×10^{18}	—	—	—	—	—
W_{DSDG}/W_{DSAG} (eV)	0.15	0.15	0.15	—	—	—	—	—
G_{MGD}/G_{MGA} (cm^{-3} eV^{-1})	—	—	—	1×10^{16}	5×10^{15}	1×10^{16}	1×10^{21}	1×10^{20}
σ_{de} (cm^2) (Gaussian)	1×10^{-14}	1×10^{-14}	1×10^{-14}	1×10^{-15}	1×10^{-14}	1×10^{-15}	1×10^{-12}	1×10^{-12}
σ_{dh} (cm^2) (Gaussian)	1×10^{-15}	1×10^{-15}	1×10^{-15}	1×10^{-17}	1×10^{-15}	1×10^{-17}	1×10^{-13}	1×10^{-13}
σ_{ae} (cm^2) (Gaussian)	1×10^{-15}	1×10^{-15}	1×10^{-15}	1×10^{-17}	1×10^{-15}	1×10^{-17}	1×10^{-13}	1×10^{-13}
σ_{ah} (cm^2) (Gaussian)	1×10^{-14}	1×10^{-14}	1×10^{-14}	1×10^{-15}	1×10^{-14}	1×10^{-15}	1×10^{-12}	1×10^{-12}

The abbreviations in Table 1 are follows : ε_r: relative permittivity, χ: electron affinity, E_G: mobility bandgap, E_{opt}: optical bandgap, d: layer thickness, N_D: donor concentration, N_A: acceptor concentration, μ_e: electron mobility, μ_h: hole mobility, N_C: effective density of states in the conduction band, N_V: effective density of states in the valance band, E_D/E_A: characteristic energy of the donor-like/acceptor-like tail states, G_{DO}/G_{AO}: exponential prefactor of donor-like/ acceptor-like tail states,σ_{de},σ_{dh}: capture cross-section for donor states, σ_{ae}, σ_{ah}: capture cross-section for acceptor states, N_{DG}/N_{AG}: Gaussian density for donor andacceptor states, W_{DSDG}/W_{DSAG}: Gaussian standard deviation for donor and acceptor, G_{MGD}/G_{MGA}: Density of midgap donor-like/acceptor-like states.

in range of 450–700 nm. The QE increases with the increase of i-layer thickness and this is due to the increase of absorption of the incident light.

In comparison with hydrogenated amorphous silicon, μc-Si:H shows no light degradation behavior. However, it has a low optical absorption and therefore i-layers have to be much thicker than amorphous i-layers [16]. Figure 5 shows the J-V characteristics under AM 1.5 illumination for μc-Si:H solar cell with different i-layer thicknesses in the range of 500–2300 nm. The V_{OC} and FF decrease with increase in thickness showing limitation of the bulk material. Besides, one can observe that the Voc of μc-Si:H is lower compared to the a-Si:H p-i-n solar cell. However, μc-Si:H exhibits higher J_{SC} for thicker i-layer, so this is can be related to an enhancement optical absorption.

Figure 6 illustrates the quantum efficiency of the μc-Si:H p-i-n solar cell. It appears clearly an enhanced response in the red and near-infrared region (600–1000 nm) in comparison with

Table 2. General layer parameters used in the simulation.

Front contact parameters		Back contact parameters	
PHIB0 (eV)	1.54	PHIBL (eV)	0.1
SNO (cm/s)	1×10^7	SLN (cm/s)	1×10^7
SPO (cm/s)	1×10^7	SPL (cm/s)	1×10^7
RF	0	RB	0.9

The abbreviations in Table 2 are follows: PHIB0/ PHIBL: barrier height, SNO/ SLN: electron recombination velocity, SPO/ SPL: hole recombination velocity, RF/ RB: reflection coefficient.

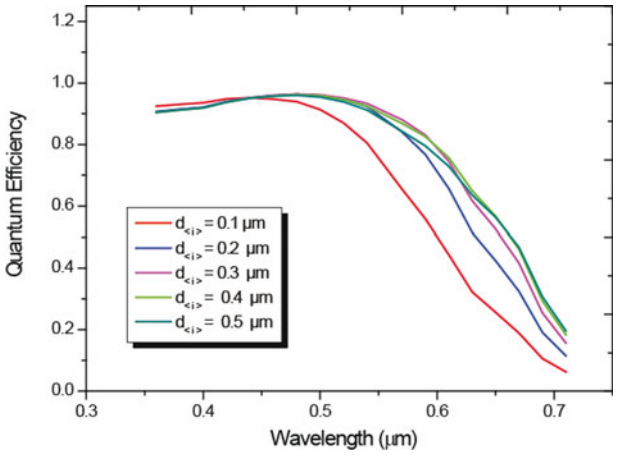

Figure 4. Quantum Efficiency (QE) characteristics of a-Si:H silicon p-i-n solar cell for different i-layer thicknesses.

amorphous p-i-n cell, this means that μc-Si:H material has a higher absorption coefficient for the longer wavelengths (red photons).

With its stability against light soaking, its low bandgap of 1.14 eV and its extended absorption in red and infrared region of the solar spectrum, μc-Si:H appears as a suitable candidate for bottom cell intrinsic material in tandem cells based amorphous solar cell [17].

3.2. *Micromorph tandem solar cell*

In our simulation, the TRJ consists of n- and p- doped microcrystalline silicon layers as shown in Fig. 2. Microcrystalline silicon has a high doping efficicency [2] and a high electrical conductivity [18], so requirements of high doping and ohmic-like behavior are fullfilled. A sufficiently high defect density is introduced in the midgap for a high recombination rate. All parameters of the TRJ are given in table 1.

Figure 7 shows the J-V characteristics of the best performing a-Si:H/μc-Si:H tandem cell (black curve) that we have obtained in comparison with the corresponding single junction

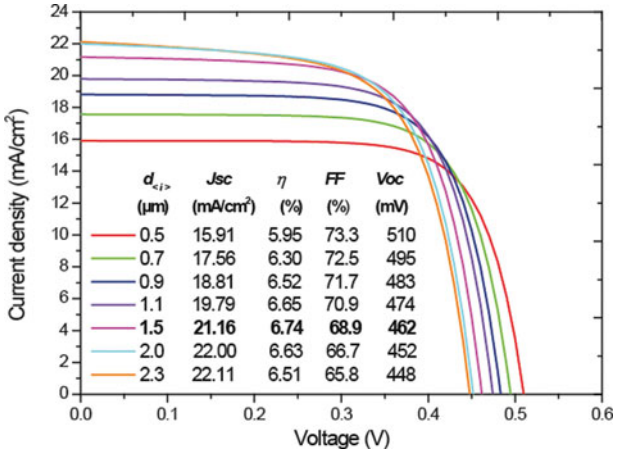

Figure 5. J-V curve under AM 1.5 illumination for μc-Si:H p-i-n solar cell for different i-layer thicknesses with output parameters.

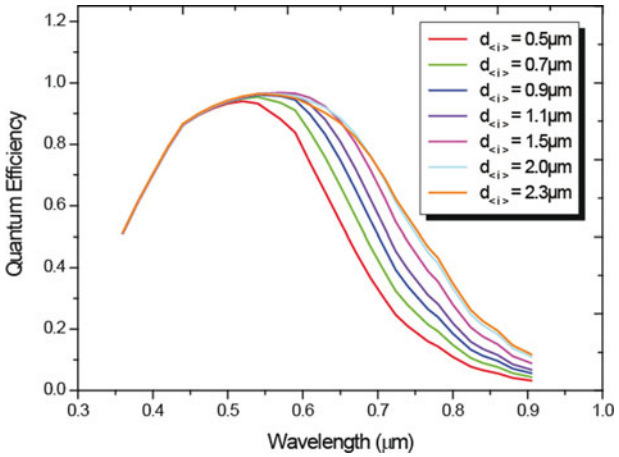

Figure 6. Quantum Efficiency (QE) characteristics of μc-Si:H p-i-n solar cell for different i-layer thicknesses.

cells. Output parameters of the micromorph and the single junctions are given in the same figure. The highest efficiency has been obtained by adjusting the thickness of the bottom i-layer while the top i-layer is kept constant at 200 nm. It reached a value of 10.46% at a bottom i-layer thickness of 2000 nm. This improvement of the efficiency is due to the enhancement of the open-circuit voltage with 1.34 V. As can be seen, this V_{OC} value is nearly equal to sum of the top and bottom cell voltages of the corresponding single junction cells ($V_{OC,top} = 923$ mV and $V_{OC,bot} = 452$ mV), showing a good series connection. Thus, we can consider that our simulated TRJ meets the requirements mentioned earlier. However, the micromorph tandem exhibits a low J_{SC} with a value of 11.41 mA/cm^2. Because of the series connection, the current density through the micromorph tandem is limited by the subcell that delivers the smallest current, so by the amorphous top cell. The ultimate requirement of higher device efficiency is an appropriate matching of the current generated in top and bottom cells [19]. One can also observe that the fill factor FF of the micromorph tandem is slighty smaller in comparison to the amorphous silicon cell.

Figure 8 illustrates the quantum efficiency curve of the micrormorph tandem solar cell. It shows a more efficient usage of the solar spectrum as compared to the single junctions.

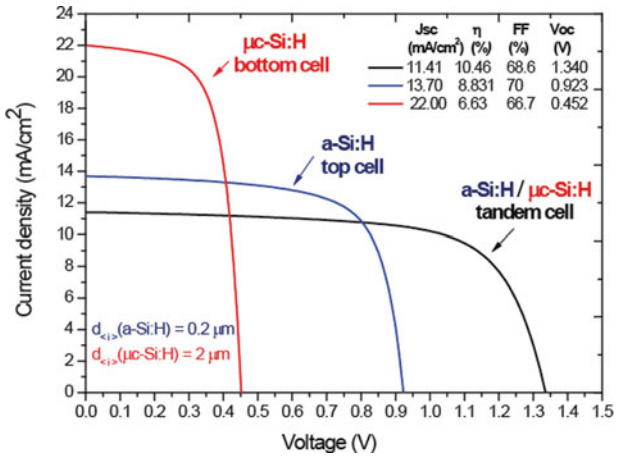

Figure 7. Comparison of the J-V curves of the best performing micromorph solar cell (black curve) with the corresponding single junction cells.

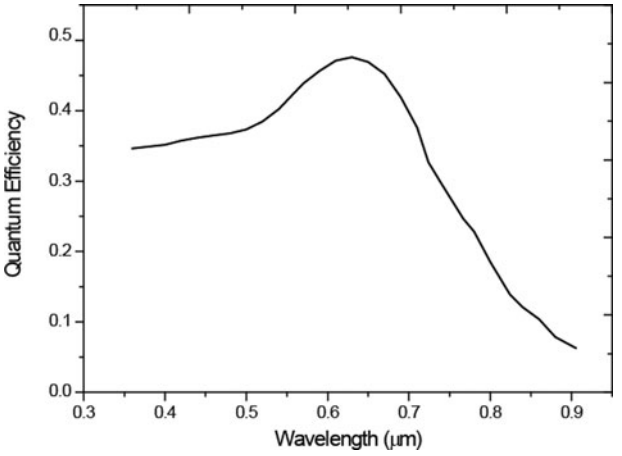

Figure 8. Quantum efficiency of the best performing micromorph tandem solar cell

Indeed, in the micromorph tandem structure, the amorphous top cell absorbs the short wavelengths whereas the transmitted long wavelengths are led to microcrystalline bottom cell.

4. Conclusions

In this work, a micromorph tandem solar cell with a microcrystalline tunnel recombination junction has been designed and optimized by using AMPS-1D software. The tunnel recombination junction is a heavily doped and highly defective np junction which creates an ohmic and low resistive electrical connection between the adjacent subcells. Our simulation results confirm the established fact that the micromorph tandem structure improves solar cell performances, leading to higher efficiencies by improving the open-circuit voltage. It has achieved the highest efficiency of 10.46% with the intrinsic top and bottom thicknesses of 200 and 2000 nm, respectively. The V_{OC} reaches 1.34V which is nearly equal to the sum of the voltages across the amorphous and microcrystalline subcells, showing a good series connection thanks to the optimized TRJ. However, the micromorph tandem solar cell delivers a low J_{SC} of 11.41 mA/cm^2. Because the series connection, the current through the tandem is limited by the subcell which generates the least current. The fill factor FF is slighty smaller in comparison with the amorphous silicon single junction. Our results are in agreement with those reported in previous works.

Acknowledgment

The authors gratefully acknowledge Pennsylvania State University, USA, for providing the AMPS-1D simulation package.

References

[1] Staebler, D. L. & Wronski, C. R. (1977). *Appl. Phys. Lett.*, *31*, 4, 292.
[2] Keppner, H., Meier, J., Torres, P., Fischer, D., & Shah, A. (1999). *Appl. Phys. Mater. Sci. Process.*, *69*, 2, 169.
[3] Guha, S., Yang, J., Banerjee, A., Glatfelter, T., & Sugiyama, S. (1997). *Sol. Energy Mater. Sol. Cells*, *48*, 1, 365.

[4] Meier, J., Keppner, H., Dubail, S., Ziegler, Y., Feitknecht, L., Torres, P., Hof, C., Kroll, U., Fischer, D., Cuperus, J., Selvan, A., & Shah, A. (1998). *2nd World Conf. Photovolt. Energy Convers.*, *I*, pp. 375–380..
[5] Meier, J., Dubail, S., Platz, R., Torres, P., Kroll, U., Anna Selvan, J. A., Pellaton Vaucher, N., Hof, C., Fischer, D., Keppner, H., Flückiger, R., Shah, A., Shklover, V., & Ufert, K.-D. (1997). *Sol. Energy Mater. Sol. Cells*, *49*, 1–4, 35.
[6] Meier, J., Dubail, S., Fluckiger, R., Fischer, D., Keppner, H., & Shah, A. (1994). vol. *1*, p. 409–412.
[7] Meier, J., Flückiger, R., Keppner, H., & Shah, A. (1994). *Appl. Phys. Lett.*, *65*, 7, 860.
[8] Chang, P.-K., Lu, C.-H., Yeh, C.-H., & Houng, M.-P. (2012). *Thin Solid Films*, *520*, 9, 3684.
[9] McElheny, J., Arch, J. K., Lin, H. S., Fonash, S. J., *J. Appl. Phys.*, *64*, 1988, 1254.
[10] Banerjee, A. & Guha, S. (1991). *J. Appl. Phys.*, *69*, 2, 1030.
[11] Belfar, A. & Aït-Kaci, H. (2012). *Thin Solid Films*, *525*, 167.
[12] Kabir, M. I., Shahahmadi, S. A., Lim, V., Zaidi, S., Sopian, K., & Amin, N. (2012). *Int. J. Photoenergy*, *2012*.
[13] Kwak, J., Kwon, S. W., & Lim, K. S. (2006). *J. Non-Cryst. Solids*, *352*, 9–20, 1847.
[14] Löffler, J., Gordijn, A., Stolk, R. L., Li, H., Rath, J. K., & Schropp, R. E. I. (2005). *Sol. Energy Mater. Sol. Cells*, *87*, 1–4, 251.
[15] Shah, A. V., Schade, H., Vanecek, M., Meier, J., Vallat-Sauvain, E., Wyrsch, N., Kroll, U., Droz, C., & Bailat, J. (2004). *Prog. Photovolt. Res. Appl.*, *12*, 2–3, 113.
[16] Shah, A. V., Meier, J., Vallat-Sauvain, E., Wyrsch, N., Kroll, U., Droz, C., & Graf, U. (2003). *Sol. Energy Mater. Sol. Cells*, *78*, 1, 469.
[17] Meier, J., Dubail, S., Golay, S., Kroll, U., Faÿ, S., Vallat-Sauvain, E., Feitknecht, L., Dubail, J., & Shah, A. (2002). *Sol. Energy Mater. Sol. Cells*, *74*, 1–4, 457.
[18] Fantoni, A., Vieira, M., & Martins, R. (1999). *Solid-State Electron.*, *43*, 9, 1709.
[19] Vetterl, O., Lambertz, A., Dasgupta, A., Finger, F., Rech, B., Kluth, O., & Wagner, H. (2001). *Solar Energy Materials and Solar Cells*, *66*, 345.